

## MALDI-TOF/TOF CID Study of Poly(*p*-phenylene sulfide) Fragmentation Reactions

Anthony P. Gies,<sup>\*,†</sup> Jon F. Geibel,<sup>‡</sup> and David M. Hercules<sup>†</sup>

<sup>†</sup>*Department of Chemistry, Vanderbilt University, Nashville, Tennessee 37235 and* <sup>‡</sup>*Chevron Phillips Chemical Company, LP, Bartlesville Technology Center, Bartlesville, Oklahoma 74004*

Received September 24, 2009; Revised Manuscript Received November 16, 2009

**ABSTRACT:** A study involving the evaporation–grinding MALDI sample preparation method, MALDI-TOF/TOF CID, and Py-GC/MS is presented to examine the fragmentation mechanisms of poly(*p*-phenylene sulfide) (PPS). MALDI-TOF/TOF CID fragmentation studies yielded a wealth of information about the mass, structure (linear or cyclic), end-groups, and backbone modifications of the polymer. Additionally, Py-GC/MS experimental data are presented for comparison of the multimolecular free radical reactions in pyrolysis with the unimolecular fragmentation reactions of MS/MS.<sup>1,2</sup> TOF/TOF CID results indicate that linear PPS undergoes random main chain fragmentation along the polymer backbone and preferentially fragments at bonds adjacent to dibenzothiophene and phenyl end-groups. Cyclic species produce fragment ions similar to linear species. However, the MS/MS precursor ions for cyclic PPS are, by far, the most intense peaks, while the precursor ions for linear species show relatively low intensity. CID fragmentation results are supported by Py-GC/MS data and are consistent with the proposed degradation mechanisms.

### Introduction

High molecular weight poly(*p*-phenylene sulfide) polymers are virtually insoluble in most solvents at ambient temperatures and, until development of the evaporation–grinding MALDI sample preparation method (E–G method),<sup>3</sup> were traditionally characterized by infrared spectrometry and thermal methods of analysis—most notably pyrolysis.<sup>4–11</sup> It should be noted that MALDI-TOF MS has the advantage of obtaining specific information about end-groups and molecular mass distributions, whereas pyrolysis-GC/MS (Py-GC/MS) is a high-energy degradation technique for identification of the polymer repeat unit and backbone architecture. When combined, these are powerful techniques for polymer analysis. However, they do have their limitations.

In previous studies of poly(*p*-phenylene sulfide) (PPS), we discussed the limits of MALDI-TOF MS, using the E–G method, for their analysis.<sup>12</sup> Briefly, MALDI-TOF MS was used to examine PPS chemistry during thermal curing and heated *N*-methyl-2-pyrrolidone (NMP) fractionation. These studies yielded information about the mass, structure, and end-groups of PPS. However, the degree of PPS cyclization, sulfoxide formation, and dibenzothiophene end-group modification was difficult to predict, and more definitive information was necessary to confirm the existence of these structures and to rule out the occurrence of isobaric PPS structures.

The current study reports a combination of MALDI-TOF/TOF CID fragmentation (using the E–G method) and Py-GC/MS to gain insight into the degradation mechanisms of PPS. The information, obtained from isolated PPS chains, was used to examine the postsynthesis modification and thermal curing of intractable poly(*p*-phenylene sulfide)s and confirm PPS chemical modifications that were proposed in our previous study.<sup>12</sup>

### Experimental Section

**Materials.** The commercial poly(*p*-phenylene sulfide) used in this study (produced by the Edmonds–Hill process<sup>13</sup>) was supplied by Chevron Phillips Chemical Co., LP, Bartlesville, OK. Cyclic-rich PPS was obtained through high-temperature GPC fractionation. The structure of the polymer repeat unit was assumed to be as shown for the cyclic species 1-1 in Table 1.

**MALDI-TOF/TOF CID Measurements.** All samples were analyzed using an Applied Biosystems 4700 Proteomics Analyzer MALDI-TOF/TOF MS (Applied Biosystems, Framingham, MA) equipped with 355 nm Nd:YAG lasers. All spectra were obtained in the positive ion mode using an accelerating voltage of 8 kV for the first source, 15 kV for the second source, and a laser intensity ~10% greater than threshold. The grid voltage, guide wire voltage, and delay time were optimized for each spectrum to achieve the best signal-to-noise ratio. The collision energy is defined by the potential difference between the source acceleration voltage and the floating collision cell; in our experiments this voltage difference was set to 1 kV. Air was used as a collision gas at pressures of  $1.5 \times 10^{-6}$  and  $5 \times 10^{-6}$  Torr (which will be referred to as “low” and “high” pressure, respectively). All spectra were acquired in the reflection mode with a mass resolution greater than 3000 fwhm; isotopic resolution was observed throughout the entire mass range detected. External mass calibration was performed using protein standards from a Sequazyme Peptide Mass Standard Kit (Applied Biosystems) and a three-point calibration method using Angiotensin I ( $m = 1296.69$  Da), ACTH (clip 1-17) ( $m = 2093.09$  Da), and ACTH (clip 18-39) ( $m = 2465.20$  Da). Internal mass calibration was subsequently performed using a PEG standard ( $M_n = 2000$ ; Polymer Source, Inc.) to yield monoisotopic mass accuracy better than  $\Delta m = \pm 0.05$  Da. The instrument was calibrated before each measurement to ensure constant experimental conditions.

All samples were run in a dithranol matrix (Aldrich) doped with silver trifluoroacetate (AgTFA, Aldrich) or copper(II) chloride (CuCl<sub>2</sub>, Aldrich) or with no cationization agent added

\*Corresponding author: Tel (615) 343-5980; e-mail a.gies@vanderbilt.edu.

**Table 1. Structural Assignments for Precursor Ion Peaks (from Figure 1) Selected for MALDI-TOF/TOF CID Fragmentation in Figures 2–5, S1, and S2**

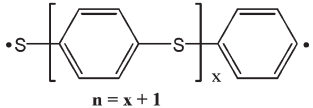
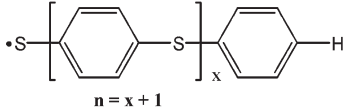
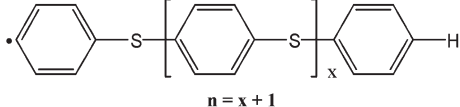
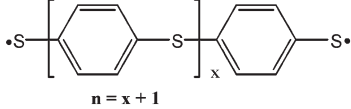
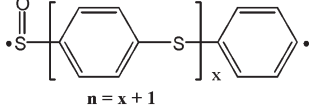
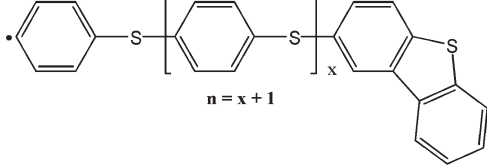
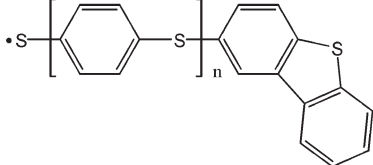
Species	Structure (M)	$\cdot^+$ M (Da)	$\text{Cu}^+$ M (Da)	$\text{Ag}^+$ M (Da)
1-1		540.0 (n = 5)	602.9 (n = 5)	646.9 (n = 5)
		648.0 (n = 6)	710.9 (n = 6)	754.9 (n = 6)
		756.0 (n = 7)	818.9 (n = 7)	862.9 (n = 7)
		864.0 (n = 8)	926.9 (n = 8)	970.9 (n = 8)
		972.0 (n = 9)	1034.9 (n = 9)	1078.9 (n = 9)
		1080.0 (n = 10)	1142.9 (n = 10)	1186.9 (n = 10)
		1188.0 (n = 11)	1250.9 (n = 11)	1294.9 (n = 11)
		1296.0 (n = 12)	1358.9 (n = 12)	1402.9 (n = 12)
		1404.0 (n = 13)	1466.9 (n = 13)	1510.9 (n = 13)
		1512.0 (n = 14)	1574.9 (n = 14)	1618.9 (n = 14)
		1620.0 (n = 15)	1682.9 (n = 15)	1726.9 (n = 15)
		.....	.....	.....
		2160.0 (n = 20)	3950.9 (n = 36)	3994.9 (n = 36)
1-2		556.0 (n = 4)	510.9 (n = 3)	554.9 (n = 3)
		664.0 (n = 5)	618.9 (n = 4)	662.9 (n = 4)
		772.0 (n = 6)	726.9 (n = 5)	770.9 (n = 5)
		880.0 (n = 7)	834.9 (n = 6)	878.9 (n = 6)
		988.0 (n = 8)	942.9 (n = 7)	986.9 (n = 7)
		1096.0 (n = 9)	1050.9 (n = 8)	1094.9 (n = 8)
		1204.0 (n = 10)	1158.9 (n = 9)	1202.9 (n = 9)
		1312.0 (n = 11)	1266.9 (n = 10)	1310.9 (n = 10)
		1420.0 (n = 12)	1374.9 (n = 11)	1418.9 (n = 11)
		1528.0 (n = 13)	1482.9 (n = 12)	1526.9 (n = 12)
		1636.0 (n = 14)	1590.9 (n = 13)	1634.9 (n = 13)
		1744.0 (n = 15)	1698.9 (n = 14)	1742.9 (n = 14)
		.....	1806.9 (n = 15)	1850.9 (n = 15)
2284.0 (n = 20)	.....	.....		
1-3		616.0 (n = 4)	679.0 (n = 4)	722.9 (n = 4)
		724.0 (n = 5)	787.0 (n = 5)	830.9 (n = 5)
		832.0 (n = 6)	895.0 (n = 6)	938.9 (n = 6)
		940.0 (n = 7)	1003.0 (n = 7)	1046.9 (n = 7)
		1048.0 (n = 8)	1111.0 (n = 8)	1154.9 (n = 8)
		1156.0 (n = 9)	1219.0 (n = 9)	1262.9 (n = 9)
		1264.0 (n = 10)	1327.0 (n = 10)	1370.9 (n = 10)
		1372.0 (n = 11)	1435.0 (n = 11)	1478.9 (n = 11)
		1480.0 (n = 12)	1543.0 (n = 12)	1586.9 (n = 12)
		1588.0 (n = 13)	1651.0 (n = 13)	1694.9 (n = 13)
		1696.0 (n = 14)	1759.0 (n = 14)	1802.9 (n = 14)
		1804.0 (n = 15)	1867.0 (n = 15)	1910.9 (n = 15)
		.....	.....	.....
2344.0 (n = 20)	2407.0 (n = 20)	2450.9 (n = 20)		
1-4		542.0 (n = 5)	604.9 (n = 5)	648.9 (n = 5)
		650.0 (n = 6)	712.9 (n = 6)	756.9 (n = 6)
		758.0 (n = 7)	820.9 (n = 7)	864.9 (n = 7)
		866.0 (n = 8)	928.9 (n = 8)	972.9 (n = 8)
		974.0 (n = 9)	1036.9 (n = 9)	1080.9 (n = 9)
		1082.0 (n = 10)	1144.9 (n = 10)	1188.9 (n = 10)
		1190.0 (n = 11)	1252.9 (n = 11)	1296.9 (n = 11)
		1298.0 (n = 12)	1360.9 (n = 12)	1404.9 (n = 12)
		1406.0 (n = 13)	1468.9 (n = 13)	1512.9 (n = 13)
		1514.0 (n = 14)	1576.9 (n = 14)	1620.9 (n = 14)
		1622.0 (n = 15)	1684.9 (n = 15)	1728.9 (n = 15)
		.....	.....	.....
		2162.0 (n = 20)	3952.9 (n = 36)	3996.9 (n = 36)

("neat"). All spectra displayed the expected mass shifts for the respective cationizing agent; AgTFA was the reagent of choice for high molecular weight PPS (1186.9 Da and above) because it yielded spectra with the best S/N ratios (S/N ratio improvement > 8%). However, low molecular weight PPS spectra displayed the best S/N ratios (> 409.5) when analyzed "neat". Samples were prepared using the evaporation–grinding (E–G) method<sup>3,14,15</sup> in which a 2 mg sample of poly(*p*-phenylene sulfide) was ground to a fine powder using an agate mortar and pestle. Then molar ratios (with respect to the moles of polymer) of 25 parts matrix and 1 part cationizing agent (if needed) were added to the finely ground polymer along with 60  $\mu\text{L}$  of distilled tetrahydrofuran (THF, Fisher). The mixture was ground until the THF evaporated, after which the residue that had accumulated on the sides of the mortar was pushed down to the bottom of the vessel. The mixture was then ground again to ensure homogeneity. A portion of the mixture was then pressed into a sample well by

spatula on the MALDI sample plate. MS and MS/MS data were processed using the Data Explorer 4.9 software (Applied Biosystems).

**Py-GC/MS Measurements.** Commercially available poly(*p*-phenylene sulfide) samples were analyzed using a Frontier Laboratories double-shot pyrolyzer (Frontier Laboratories, Japan) interfaced to a Hewlett-Packard 5890 II gas chromatograph and a Hewlett-Packard 5970 mass selective detector (electron ionization = 70 eV). Platinum cups were used to ensure homogeneous heating of the sample. Pyrolysis was performed using the following protocol: 0.5 mg of polymer was placed into a platinum sample cup and allowed to purge under a 100 mL/min flow of 99.999% pure (grade 5) helium for 3 min inside the upper "cool" stage of the pyrolyzer. The pyrolyzer furnace was then heated to 500  $^{\circ}\text{C}$ , the sample cup "dropped" into the furnace, and a GC/MS was taken of the pyrolysis products. After obtaining the GC/MS, the sample

Table 2. Structural Assignments for Fragment Peaks in the MALDI-TOF/TOF CID Mass Spectra Reported in Figures 2–5, S1, and S2

Species	Structure (M)	*+ (* = Carbocation with no Ag <sup>+</sup> or Cu <sup>+</sup> ) M (Da)
2-PS		108.0 (n = 1) 216.0 (n = 2) 324.0 (n = 3) 432.0 (n = 4) 540.0 (n = 5) ..... 1080.0 (n = 10) 1188.0 (n = 11)
2-HPS		109.0 (n = 1) 217.0 (n = 2) 325.0 (n = 3) 433.0 (n = 4) 541.0 (n = 5) ..... 1081.0 (n = 10) 1189.0 (n = 11)
2-PP		184.0 (n = 1) 292.0 (n = 2) 400.0 (n = 3) 508.0 (n = 4) 616.0 (n = 5) ..... 1156.0 (n = 10) 1264.0 (n = 11)
2-HPP		185.0 (n = 1) 293.0 (n = 2) 401.0 (n = 3) 509.0 (n = 4) 617.0 (n = 5) ..... 1157.0 (n = 10) 1265.0 (n = 11)
2-SS		140.0 (n = 1) 248.0 (n = 2) 356.0 (n = 3) 464.0 (n = 4) 572.0 (n = 5) ..... 1112.0 (n = 10) 1220.0 (n = 11)
2-PSO		124.0 (n = 1) 232.0 (n = 2) 340.0 (n = 3) 448.0 (n = 4) 556.0 (n = 5) ..... 1096.0 (n = 10) 1204.0 (n = 11)
2-DP		291.0 (n = 1) 399.0 (n = 2) 507.0 (n = 3) 615.0 (n = 4) 723.0 (n = 5) ..... 1263.0 (n = 10) 1371.0 (n = 11) 1479.0 (n = 12) 1587.0 (n = 13)
2-DS		323.0 (n = 1) 431.0 (n = 2) 539.0 (n = 3) 647.0 (n = 4) 755.0 (n = 5) ..... 1295.0 (n = 10) 1403.0 (n = 11) 1511.0 (n = 12) 1619.0 (n = 13)

cup was removed from the pyrolyzer furnace and flame-cleaned while the furnace temperature was raised 50 °C. This procedure was repeated using a new sample until a furnace

temperature of 700 °C was reached. Product separation was performed using a 30 m (0.25 mm i.d. and 0.25 μm film thickness) SupelcoWax-10 capillary column (Supelco,

**Table 3. Comparison of the Fragment Ions Identified in the MALDI-TOF/TOF CID Mass Spectra Reported in Figures 2–5 and S2**

fragment species	Figure 2	Figure 3	Figure 4		Figure 5		Figure S2
	species 1-1 M* <sup>+</sup> (Da) (major)	species 1-1 M <sup>Ag+</sup> (Da) (major)	species 1-2 M* <sup>+</sup> (Da) (major)	species 1-3 M* <sup>+</sup> (Da) (minor)	species 1-3 M* <sup>+</sup> (Da) (major)	species 1-2 M* <sup>+</sup> (Da) (minor)	species 1-3 M* <sup>+</sup> (Da) (major)
*2-PS	108.0 ( <i>n</i> = 1) 216.0 ( <i>n</i> = 2) 324.0 ( <i>n</i> = 3) 432.0 ( <i>n</i> = 4) 540.0 ( <i>n</i> = 5) 648.0 ( <i>n</i> = 6) 756.0 ( <i>n</i> = 7) 864.0 ( <i>n</i> = 8) 972.0 ( <i>n</i> = 9)	216.0 ( <i>n</i> = 2) 324.0 ( <i>n</i> = 3) 432.0 ( <i>n</i> = 4) 540.0 ( <i>n</i> = 5) 648.0 ( <i>n</i> = 6) 756.0 ( <i>n</i> = 7) 864.0 ( <i>n</i> = 8) 972.0 ( <i>n</i> = 9) 1080.0 ( <i>n</i> = 10) 1188.0 ( <i>n</i> = 11)	324.0 ( <i>n</i> = 3) 432.0 ( <i>n</i> = 4) 540.0 ( <i>n</i> = 5) 648.0 ( <i>n</i> = 6) 756.0 ( <i>n</i> = 7) 864.0 ( <i>n</i> = 8) 972.0 ( <i>n</i> = 9) 1080.0 ( <i>n</i> = 10)	X	X	432.0 ( <i>n</i> = 4) 540.0 ( <i>n</i> = 5) 648.0 ( <i>n</i> = 6) 756.0 ( <i>n</i> = 7) 864.0 ( <i>n</i> = 8) 972.0 ( <i>n</i> = 9) 1080.0 ( <i>n</i> = 10) 1188.0 ( <i>n</i> = 11)	216.0 ( <i>n</i> = 2) 324.0 ( <i>n</i> = 3) 432.0 ( <i>n</i> = 4) 540.0 ( <i>n</i> = 5) 648.0 ( <i>n</i> = 6) 756.0 ( <i>n</i> = 7) 864.0 ( <i>n</i> = 8) 972.0 ( <i>n</i> = 9) 1080.0 ( <i>n</i> = 10) 1188.0 ( <i>n</i> = 11) 1296.0 ( <i>n</i> = 12) 1404.0 ( <i>n</i> = 13)
*2-HPS	X	X	X	217.0 ( <i>n</i> = 2) 1081.0 ( <i>n</i> = 10) 1189.0 ( <i>n</i> = 11)	217.0 ( <i>n</i> = 2) 325.0 ( <i>n</i> = 3) 1189.0 ( <i>n</i> = 11) 1297.0 ( <i>n</i> = 12)	X	1405.0 ( <i>n</i> = 13) 1513.0 ( <i>n</i> = 14)
*2-PP	184.0 ( <i>n</i> = 1) 292.0 ( <i>n</i> = 2) 400.0 ( <i>n</i> = 3) 508.0 ( <i>n</i> = 4) 616.0 ( <i>n</i> = 5) 724.0 ( <i>n</i> = 6) 832.0 ( <i>n</i> = 7) 940.0 ( <i>n</i> = 8)	184.0 ( <i>n</i> = 1) 292.0 ( <i>n</i> = 2) 400.0 ( <i>n</i> = 3) 508.0 ( <i>n</i> = 4) 616.0 ( <i>n</i> = 5) 724.0 ( <i>n</i> = 6) 832.0 ( <i>n</i> = 7) 940.0 ( <i>n</i> = 8) 1048.0 ( <i>n</i> = 9) 1156.0 ( <i>n</i> = 10)	508.0 ( <i>n</i> = 4) 616.0 ( <i>n</i> = 5) 724.0 ( <i>n</i> = 6) 832.0 ( <i>n</i> = 7) 940.0 ( <i>n</i> = 8) 1048.0 ( <i>n</i> = 9) 1156.0 ( <i>n</i> = 10)	X		184.0 ( <i>n</i> = 1) 292.0 ( <i>n</i> = 2) 400.0 ( <i>n</i> = 3) 508.0 ( <i>n</i> = 4) 616.0 ( <i>n</i> = 5) 724.0 ( <i>n</i> = 6) 832.0 ( <i>n</i> = 7) 940.0 ( <i>n</i> = 8) 1048.0 ( <i>n</i> = 9) 1156.0 ( <i>n</i> = 10)	184.0 ( <i>n</i> = 1) 292.0 ( <i>n</i> = 2) 400.0 ( <i>n</i> = 3) 508.0 ( <i>n</i> = 4) 616.0 ( <i>n</i> = 5) 724.0 ( <i>n</i> = 6) 832.0 ( <i>n</i> = 7) 940.0 ( <i>n</i> = 8) 1048.0 ( <i>n</i> = 9) 1156.0 ( <i>n</i> = 10) 1264.0 ( <i>n</i> = 11)
*2-HPP	X	X	X	X	293.0 ( <i>n</i> = 2) 401.0 ( <i>n</i> = 3) 509.0 ( <i>n</i> = 4)	X	X
*2-SS	572.0 ( <i>n</i> = 5) 678.0 ( <i>n</i> = 6) 788.0 ( <i>n</i> = 7) 896.0 ( <i>n</i> = 8)	X	X	X	X	X	X
*2-PSO	X	X	340.0 ( <i>n</i> = 3) 448.0 ( <i>n</i> = 4) 556.0 ( <i>n</i> = 5) 664.0 ( <i>n</i> = 6) 772.0 ( <i>n</i> = 7) 880.0 ( <i>n</i> = 8) 988.0 ( <i>n</i> = 9) 1096.0 ( <i>n</i> = 10) 1204.0 ( <i>n</i> = 11) 1204.0 ( <i>n</i> = 11)	X	X	556.0 ( <i>n</i> = 5) 664.0 ( <i>n</i> = 6) 772.0 ( <i>n</i> = 7) 880.0 ( <i>n</i> = 8) 988.0 ( <i>n</i> = 9) 1096.0 ( <i>n</i> = 10) 1204.0 ( <i>n</i> = 11) 1312.0 ( <i>n</i> = 12) 1420.0 ( <i>n</i> = 13)	X
*2-DP	X	X	X	1155.0 ( <i>n</i> = 9)	291.0 ( <i>n</i> = 1) 1371.0 ( <i>n</i> = 11)	X	1479.0 ( <i>n</i> = 12) 1587.0 ( <i>n</i> = 13)
*2-DS	X	X	X	1079.0 ( <i>n</i> = 8) 1187.0 ( <i>n</i> = 9)	1295.0 ( <i>n</i> = 10) 1403.0 ( <i>n</i> = 11)	X	1511.0 ( <i>n</i> = 12) 1619.0 ( <i>n</i> = 13)

Bellefonte, PA) and the following GC/MS heating program: start at 50 °C and ramp at 5.0 °C/min for 46.0 min before finally holding at 280 °C for 9.0 min, for a total GC/MS heating cycle of 55.0 min.<sup>16</sup>

## Results and Discussion

This study reports a series of experiments which were conducted to evaluate the usefulness of mass spectrometry for studying the Edmonds–Hill process for producing high-MW poly(*p*-phenylene sulfide) (PPS). The focus of this paper will be on combining the PPS chemistry learned through MALDI-TOF/TOF CID fragmentation of various cyclic and linear low molecular weight oligomers with the information obtained from Py-GC/MS fragmentation of high MW PPS. Specifically, MALDI-TOF/TOF CID data presented will examine the selectively extracted low molecular weight (cyclic and end-group rich) portion of PPS,<sup>17</sup> and Py-GC/MS data will examine the entire mass range of the PPS sample.

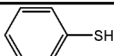
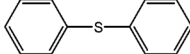
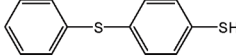
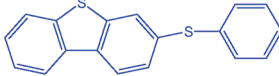
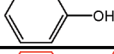
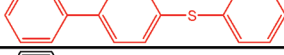
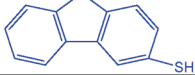
Previous Py-GC/MS studies have reported general mechanistic information for the thermal degradation of PPS,<sup>4–11</sup> but to

date none has compared PPS data from the multimolecular free radical reactions of Py-GC/MS with data from the unimolecular fragmentation of MS/MS. More importantly, no previous studies reported species specific fragmentation mechanisms or provided end-group information, both of which are described in detail in this study. We will first define our nomenclature for PPS MALDI spectra and fragmentation reactions. This will be followed by a description of TOF/TOF CID fragmentation and Py-GC/MS data. Finally, an overall mechanistic model will be proposed which explains the products observed in both TOF/TOF CID and pyrolysis. Additional poly(*p*-phenylene sulfide) TOF/TOF CID fragmentation spectra are provided as Supporting Information to further verify the peak assignments by following the fragmentation of each precursor ion to its next higher or lower number of repeat units (*n*).

**Nomenclature.** *Terminology.* Figures, tables, and schemes will show structures and mass peaks labeled according to the following key:

(i) Precursor and fragment ion peaks (Tables 1–3) and pyrolysis products (Table 4) are all labeled in the *x-y* format

Table 4. Structural Assignments for Pyrolysis Products Observed in the Py-GC/MS Pyrograms Reported in Figure 6

Species	Ret. Time (min)	Structure (M)	M (Da) (* = no Ag <sup>+</sup> )	Peak Intensity (% Base Peak)
4-1	10.39		*110.0	100 - <u>Major</u>
4-2	24.17		*186.1	32.2 - <u>Medium</u>
4-3	44.70		*294.1	31.6 - <u>Medium</u>
4-4	29.25		*184.0	13.6 - <u>Small</u>
4-5	33.17		*218.0	7.2 - <u>Small</u>
4-6	54.99		*292.0	7.0 - <u>Small</u>
4-7	1.69		*34.0	6.0 - <u>Minor</u>
4-8	19.51		*94.0	5.4 - <u>Minor</u>
4-9	39.91		*262.1	4.4 - <u>Minor</u>
4-10	2.66		*78.1	4.3 - <u>Minor</u>
4-11	46.49		*260.1	2.4 - <u>Trace</u>
4-12	37.71		*216.0	1.8 - <u>Trace</u>
4-13	21.14		*142.0	1.5 - <u>Trace</u>
4-14	19.49		*124.0	1.1 - <u>Trace</u>
4-15	19.12		*154.1	0.4 - <u>Trace</u>
4-16	29.12		*186.1	0.2 - <u>Trace</u>

where  $x$  = table number,  $y$  = structure number for precursor ions and structure letters for fragment ions. For MALDI, the table and structure number are followed by the ion which provides the charge added to the oligomers during the MALDI process (e.g., Cu<sup>+</sup>, Ag<sup>+</sup>, or "\*" for a carbocation). For convenience, in Figures 2–6 we have inserted the precursor ion structures above the corresponding CID fragmentation mass spectrum, along with mass numbers of ions formed by specific bond fragmentation.

(ii) Fragment ion end-group or main-chain modification (listed in Table 2) where P = a phenyl end-group, S = a sulfur end-group, D = a dibenzothiophene end-group, SO = a sulfoxide end-group or sulfoxide main-chain modification to a sulfur-capped species, and H = a hydrogen atom attached to a phenyl end-group. To avoid confusion with precursor ion and fragment ion peaks, CID fragment ions are identified based on their end-groups, e.g., 2-PS in Table 2.

(iii) The number of repeat units ( $n$ ) which corresponds to the mass numbers found in Tables 1–3.

For example, a precursor ion peak labeled "1-2 Cu<sup>+</sup>" corresponds to structure 1-2 in Table 1 with copper

cationization (Cu<sup>+</sup>) and some number ( $n$ ) of PPS repeat units. Similarly, a CID fragment peak labeled "\*2-PS<sub>5</sub>" corresponds to the PPS radical fragment 2-PS, shown in Table 2, which has a phenyl group on one chain end and a sulfur group on the other chain end; it is a carbocation (\*) having five PPS repeat units ( $n = 5$ ). The structures of the fragment ions identified in Figures 2–6 are given in Table 2. The mass ranges are listed for ions having different  $n$  values with the highest mass peak observed for a series listed at the bottom of the series.

**Fragmentation Model for Poly(*p*-phenylene sulfide).** It is important to stress that the production of PPS CID fragment ions depends primarily on the extent of precursor ion "damage" caused by impact with the collision gas. For example, a glancing blow will only impart a small portion of the collision energy into the PPS molecule and result in little, if any, fragmentation. However, a direct impact will be sufficiently energetic to cause multiple chain breaks, followed by extensive secondary reactions. Keeping this in mind, we will now briefly describe the different bond-breaking reactions for PPS and use them later to describe the fragment ion series observed in Figures 2–6.

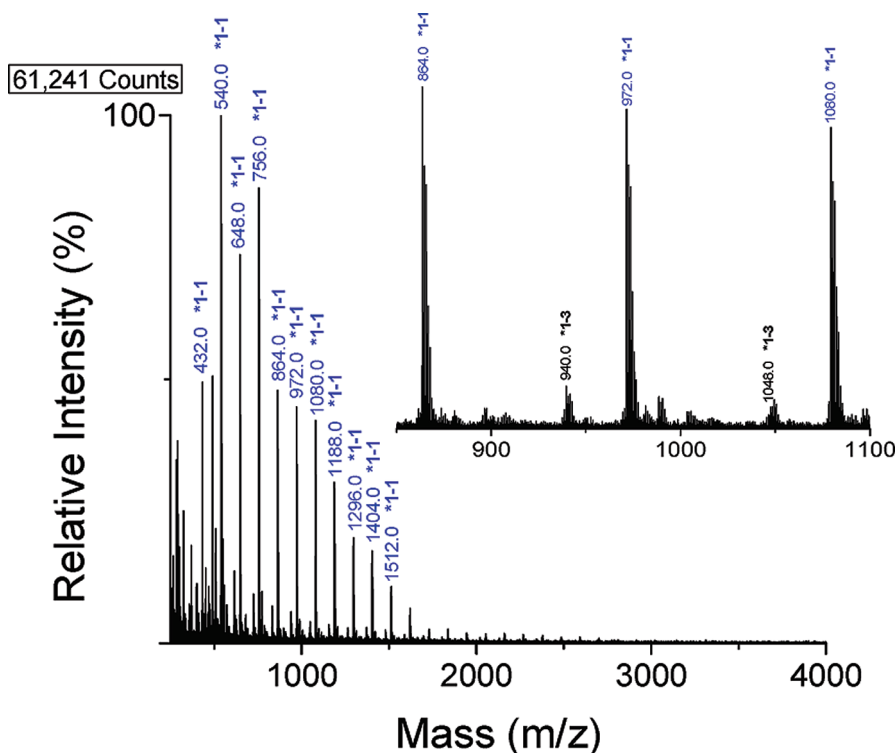


**Figure 1.** MALDI-TOF mass spectrum (mass range 250–4000 Da) of NMP isolated cyclic-rich PPS. The insert covers two repeat units, 850–1100 Da. Sample prepared by the E–G method in dithranol; no cationization agent was added.

#### Initial Bond-Breaking Reactions

**Single Chain Break.** Cyclic PPS (e.g., species \*1-1,  $n = 9972$  Da) can undergo a single bond break (Scheme 1Ai) to produce a linear species (\*2-PS<sub>9</sub>). Because this linear species is isobaric with its cyclic precursor, it can provide no information about the structure of the PPS molecule. Cyclic species require a minimum of two main-chain bond breaks to yield useful CID fragmentation data. However, linear molecules only require a single main-chain break to produce usable CID spectra.

**Multiple Chain Breaks.** When the linear fragment ion from Scheme 1Ai (species \*2-PS<sub>9</sub>) undergoes additional main-chain fragmentation, a variety of smaller fragment ions can be produced as shown in Schemes 1Aii and 1Aiii: (1Aii) \*2-PP<sub>*n*</sub> and \*2-SS<sub>*n*</sub> and (1Aiii) \*2-PS<sub>*n*</sub>. Statistically, the number of \*2-PS species produced will equal the sum of the other two. It is assumed that the charge site will be randomly distributed among sulfur atoms along the chain. It is possible that the species formed initially (2-PS, 2-PP, 2-SS) can undergo further fragmentation, as shown in Scheme 2. Species 2-PP and 2-SS can produce only two types of fragments each, but 2-PS can produce three. Therefore, overall, these reactions will not change the statistical distribution of species from that of the initial chain fragmentation.

Another possibility that must be considered is loss of neutral molecules from the fragment species. One possibility would be loss of 1,4-dithiobenzoquinone (DTQ) from the sulfur-terminated species, 2-PS and 2-SS, as shown in Scheme 2Di. Other possibilities would be loss of Ph or Ph-S neutral radicals. These possibilities will be considered subsequently.

**End-Group Fragmentation in Linear PPS.** Linear PPS oligomers show preferential loss of end-groups in MALDI CID, as shown in Scheme 1B. This topic will be addressed in the detailed discussion of their CID spectra.

**MALDI-TOF/TOF CID.** By correlating the results of MALDI-TOF MS and collision-induced dissociation (CID), structural information about polymers can be determined from fragment peaks of precursor ions along with identification of end-groups. MALDI-TOF MS was initially performed on each sample to determine the “ideal” peak series for CID fragmentation. Figure 1 shows a MALDI spectrum of a typical PPS sample. The major species are cyclic oligomers (structure 1-1 in Table 1) ranging from 5 to 20 repeat units. Also listed in Table 1 are the masses of the individual oligomers both for metal cationization and for “neat” carbocations. The inset in Figure 1 shows two major oligomer peaks (1-1) and the presence of linear oligomers (1-3), the latter having 4–20 repeat units. CID fragmentation was performed on cyclic PPS oligomer ions extracted from the MALDI spectrum, for example, the 972 Da species shown in Figure 2. The low effective kinetic energy for fragmentation of our TOF/TOF CID instrument limited CID measurements to the lower molecular weight portion of the PPS molecular mass distribution—molecular masses above 2000 Da did not generate usable CID spectra for PPS. As typical examples, we will focus our discussion on the fragmentation of the cyclic uncationized PPS oligomer (1-1) at 972.0 Da ( $n = 9$ ) shown in Figure 2; on a Ag-cationized cyclic PPS oligomer at 1294.9 Da, shown in Figure 3; on a Cu-cationized sulfoxide modified cyclic species (1-2) at 1267.0 Da ( $n = 11$ ) as shown in Figure 4; and on a dibenzothiophene–phenyl-capped linear species (1-3) at 1480.0 Da ( $n = 12$ ) shown in Figure 5. Table 2 summarizes the range of masses for the fragment ion peak series observed in MALDI-TOF/TOF CID mass spectra from cyclic and linear PPS oligomer ions. All values listed are for PPS carbocations (no cationizing agent was added), unless noted otherwise. The values given are limited in two ways. First, only fragment peaks lower than the parent ion mass can be observed for a given oligomer. Second, because of S/N

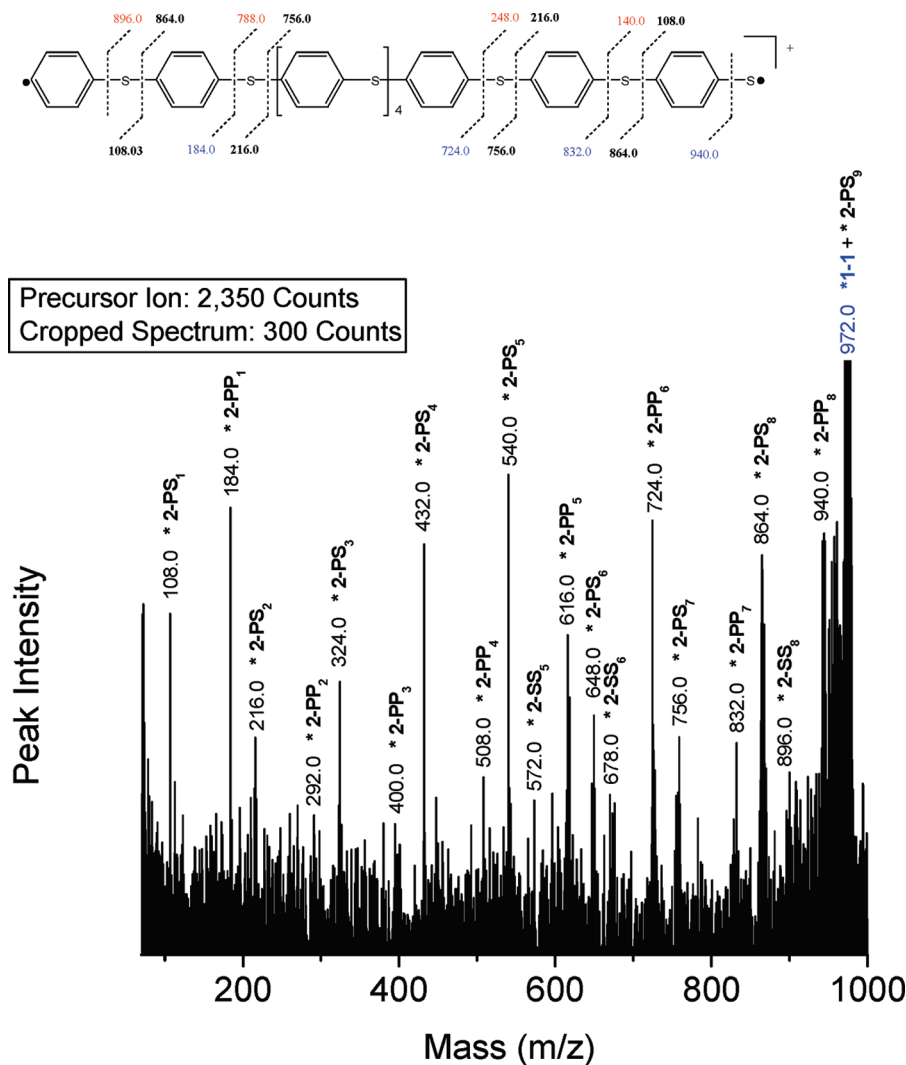


**Figure 2.** MALDI-TOF/TOF mass spectrum for cyclic PPS species 1-1 (972.0 Da precursor ion) at a low collision gas pressure of  $1.5 \times 10^{-6}$  Torr. Precursor ion cationization is through carbocation formation. Please note that the precursor ion is the most intense peak in the mass spectrum (base peak). Also, this spectrum has been cropped from 2350 counts (precursor ion) to 300 counts, to emphasize the fragment ion peaks. These definitions also apply to Figures 3–5.

issues, not all possible peaks were necessarily observed in every spectrum.

MS/MS allows the study of unimolecular polymer degradation in which an array of fragment ion masses is detected in one single, highly resolved spectrum.<sup>18</sup> The bond dissociation energies in the polysulfides are Ph–S (66 kcal/mol), Ph–H (99 kcal/mol), and C–C (114 kcal/mol).<sup>19</sup> Therefore, fragmentation should involve radicals formed by the cleavage of a Ph–S bond. On the basis of Py-GC/MS results<sup>11</sup> (*vide infra*), one also would expect random CID fragmentation of the Ph–S bonds along the PPS backbone. The CID “pulse” input of kinetic energy is much shorter in duration than the continuous kinetic energy supplied in Py-GC/MS; therefore, fragmentation in CID should be much less extensive and produce larger fragments. Furthermore, CID fragments generally contain intact polymer end-groups.<sup>18,20,21</sup>

**PPS Precursor Species 1-1.** Figure 2 shows the MALDI-TOF/TOF CID spectrum for the cyclic PPS species with  $n = 9$  (species \*1-1: 972.0 Da). The precursor ion was selected from the MALDI spectrum shown in Figure 1. The TOF/TOF fragmentation spectrum (Figure 2) indicates that cyclic PPS randomly fragments along the Ph–S chain, as expected, generating primarily phenyl–sulfur (PS) and

phenyl–phenyl (PP) capped fragments, with only small amounts of sulfur–sulfur (SS) end-capped species. Using this information, it was possible to generate a general fragmentation mechanism for cyclic PPS species as shown in Scheme 1.

The peak seen at 972 Da in Figure 2 is from the precursor ion and is (typically) the most intense peak in the CID spectrum. The intensity scale has been cropped to enhance the fragment ion intensities. Three fragment species are observed: \*2-PP, \*2-PS, and \*2-SS. The structures of these species are given in Table 2. A summary of the specific fragments observed in Figure 2 is presented in Table 3. It is important to note that the \*2-PS and \*2-PP fragment ion peaks are major fragment peaks observed in the CID spectrum, as predicted by our fragmentation mechanism. However, species \*2-SS are grossly underrepresented in our spectra. The 2-PS species account for about 50% of the total ion current observed for the three types of fragment ion peaks, and the 2-PP species account for about 42%. The 2-SS species account for only about 8%.

From Figure 2 and Table 3 it is evident that all requisite fragment ions for 2-PS and 2-PP generated by CID of the 972 Da 1-1 species are observed for the series  $n = 1–8$ . However, only three members of the 2-SS series are

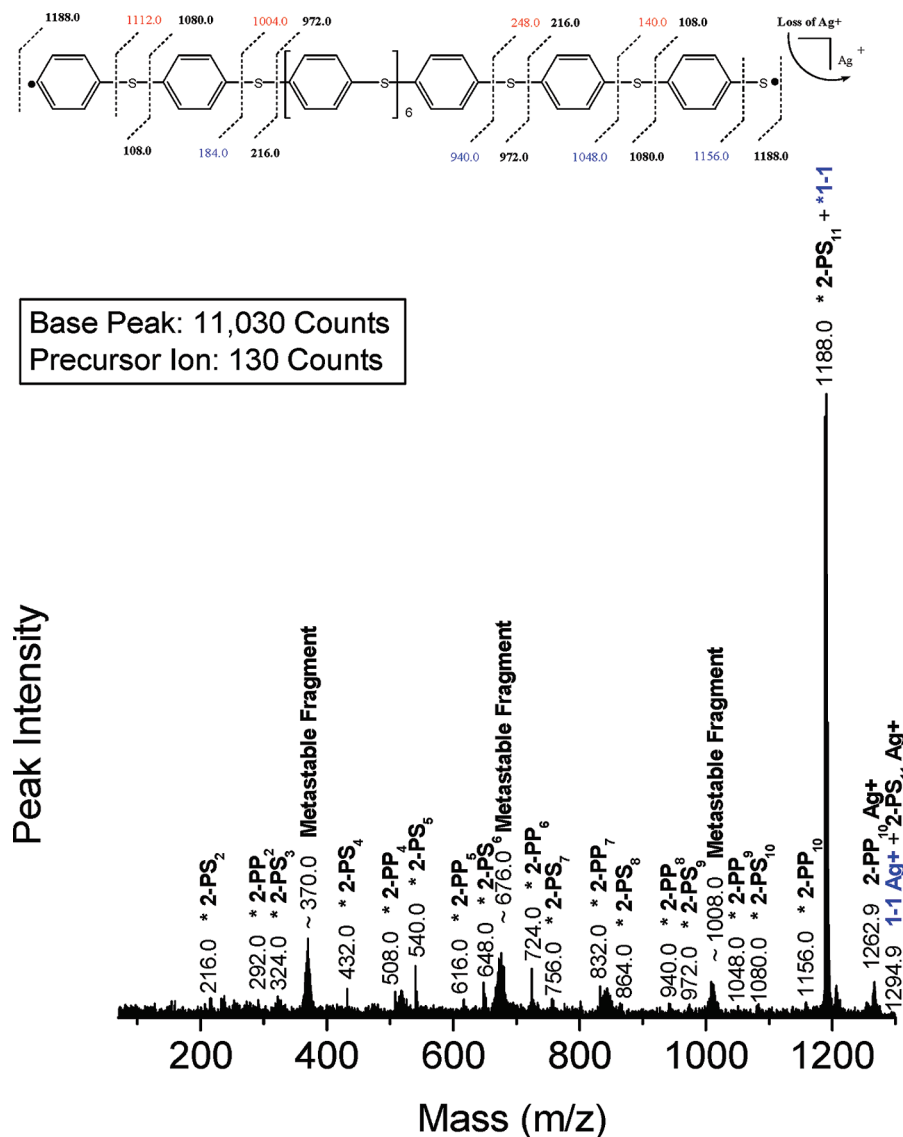


**Figure 3.** MALDI-TOF/TOF mass spectrum for cyclic PPS species 1-1 (1294.9 Da precursor ion) at a low collision gas pressure of  $1.5 \times 10^{-6}$  Torr. Precursor ion is through  $\text{Ag}^+$  cationization. Please note that the base peak (1188.0 Da) is the precursor ion minus the silver cation ( $M - 106.9$  Da). This mass spectrum has *not* been cropped.

evident ( $n = 5, 6,$  and  $8$ ). Both 2-PS and 2-PP show species with  $n = 5$  or  $n = 6$  as the most intense peaks for all spectra we studied. On a strictly statistical basis, one would anticipate that  $\sim 50\%$  of the total ion current would come from 2-PS and 25% each from 2-PP and 2-SS. The logic behind this can be seen from Schemes 1Aii and 1Aiii. Random fragmentation of Ph-S bonds along the chain (and random charge distribution) will produce 2 PS species, 1 PP, and 1 SS for a single chain fracture. If it is assumed that phenyl-terminated species are essentially stable, but that S-terminated groups are not, and that loss of 1,4-dithiobenzoquinone (DTQ) is a major fragmentation pathway, it is possible to create a scheme that fits the observed ion-current intensities. Scheme 3 summarizes the arguments. If we assume that DTQ loss is the major fragmentation pathway for S-terminated species, then loss of DTQ from PS will produce PP and, similarly, loss from SS will produce PS. Because SS is twice as likely as PS to fragment by this pathway, SS will produce an amount of PS equal to the PS lost to PP production. In the example given in Scheme 3E, it is assumed (for argument) 30% of PP is lost by this route and 60% by SS. The net effect will be

accumulation of PP, which is what is seen in the total ion current.

An interesting effect was observed in the MALDI CID of the Ag-cationized cyclic PPS. Figure 3 shows the CID spectrum obtained for the Ag-cationized oligomer,  $n = 11$ , 1294.9 Da. Surprisingly the major peak in the spectrum is at 1188.0 Da, the mass of the uncationized oligomer. This means that silver cationized cyclic PPS does not retain its silver cation during CID fragmentation. Instead, the silver cation is lost, but the charge is retained on the (presumably) linear PPS by carbocation formation. In other words, the Ag is reduced to its elemental form by the collision. Compare the peak intensities of fragment ion  $*2\text{-PS}_{11}$  ( $m/z = 1188.0$ ) vs the precursor ion (1-1  $m/z = 1294.9$ ), in Figure 3, with the comparable peaks in Figure 2. The parent/fragment ion ratios of the two differ significantly. This result argues strongly that the Ag is attached to a sulfur atom in the cyclic oligomer. The same effect was observed for cyclic PPS species cationized with Cu. The other fragment-ion peaks observed in the CID spectrum are weak relative to the 1188.0 Da peak, but are those that would be expected on the basis of Figure 2; all requisite 2-PS and 2-PP peaks are observed

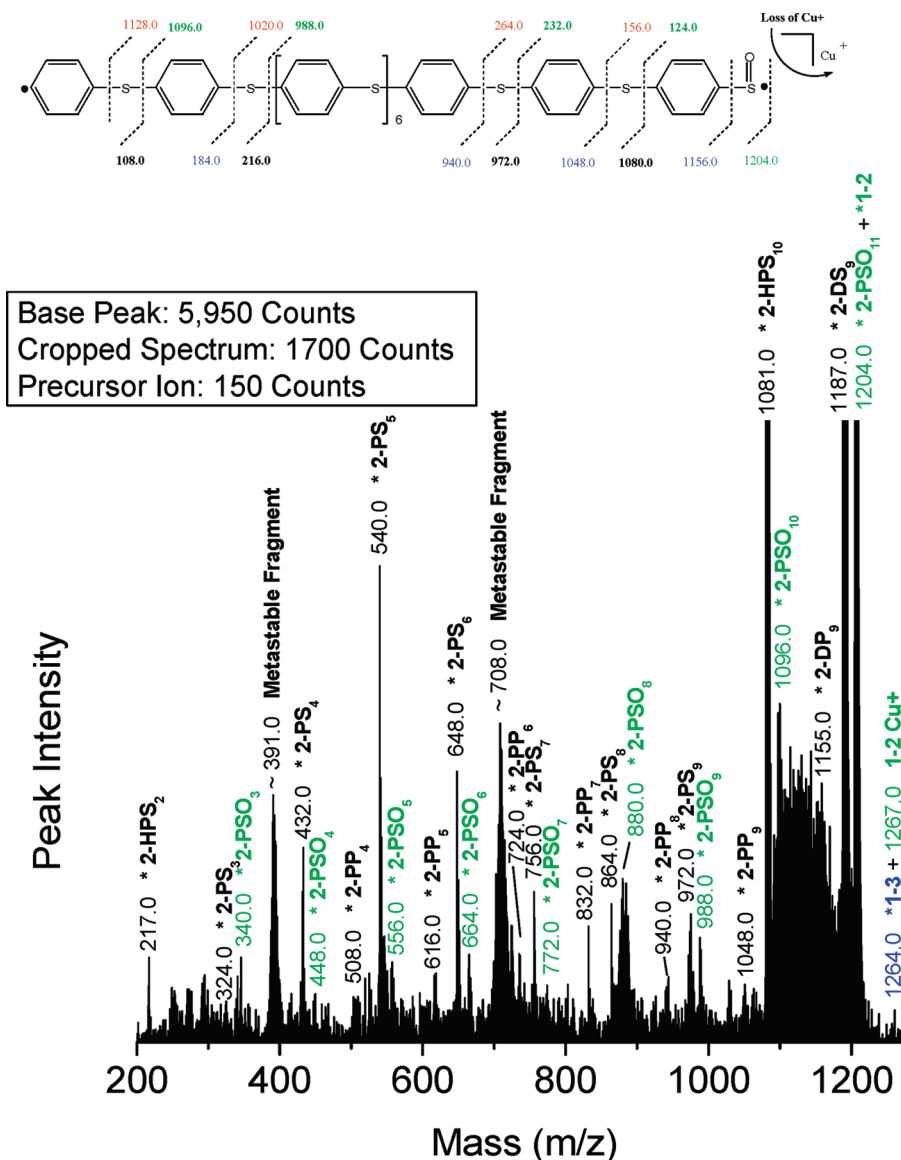


**Figure 4.** MALDI-TOF/TOF mass spectrum for sulfoxide containing cyclic PPS species 1-2 (1267.0 Da precursor ion) at a low collision gas pressure:  $1.5 \times 10^{-6}$  Torr. Precursor ion is through cationization by  $\text{Cu}^+$ . There is also a small portion of carbocationized species 1-3 present in the spectrum. Please note that the base peak is a fragment ion peak (1081.0 Da), produced by loss of a dibenzothiophene end-group from the second precursor ion at 1264.0 Da ( $M - 183$  Da). Also, this spectrum has been cropped from 5950 counts (base peak) to 1700 counts, to emphasize the fragment ion peaks.

except for the  $n = 3$  2-PP peak at 400 Da. No 2-SS peaks are evident. A number of significant metastable peaks appear in the spectrum.

**PPS Precursor Species 1-2.** Figure 4 shows the MALDI-TOF/TOF CID spectrum for cyclic, sulfoxide containing, species of PPS (species 1–2  $\text{Cu}^+$ : 1267.0 Da). It is important to note that these are copper cationized species. Because of copper cationization, these cyclic species produce a distinct fragmentation pattern that can be differentiated from the dibenzothiophene–phenyl-capped linear PPS species (species \*1-3: 1264.0 Da), which also appear in this spectrum. For example, by phenomena previously mentioned, the large peak at 1204.0 Da (\*2-PSO<sub>11</sub>) is produced by carbocationized cyclic species (species \*1-2), which are formed after the precursor ion lost the copper cation ( $M - \text{Cu}^+$ ). Also, since this is a cyclic species, the molecular ion will be most intense because multiple chain breaks are required to produce usable fragment peaks.

Using the species specific fragmentation mechanism, shown at the top of Figure 4, we will now verify the presence

of a sulfoxide containing species. Working from right-to-left through (the top row of mass numbers) the predicted fragment ions in Figure 4, we can identify peaks at  $m/z = 340.0$  (\*2-PSO<sub>3</sub>), 448.0 (\*2-PSO<sub>4</sub>), 556.0 (\*2-PSO<sub>5</sub>), 664.0 (\*2-PSO<sub>6</sub>), 772.0 (\*2-PSO<sub>7</sub>), 880.0 (\*2-PSO<sub>8</sub>), 988.0 (\*2-PSO<sub>9</sub>), 1096.0 (\*2-PSO<sub>10</sub>), and 1204.0 (\*2-PSO<sub>11</sub>). A summary of these fragment peaks is presented in Table 3 for comparison with fragment ions observed in Figures 2, 3, 5, and 6. Working from left-to-right (the bottom row of mass numbers), simply identifies mass peaks formed by fragment ions from species 1-2 and 1-3. Since, the majority of the fragment ion peaks for species 1-2 and 1-3 are isobaric, the most definitive peaks for the identification of species 1-2 are those which contain a sulfoxide group (i.e., the mass peaks labeled \*2-PSO) or represent the loss of a copper ion (e.g., \*2-PSO<sub>11</sub>;  $m/z = 1204.0$ ); for species 1-3, the most definitive fragment peaks are represented by the loss of a dibenzothiophene end-group (e.g., \*2-HPS<sub>10</sub>;  $m/z = 1081.0$ ) and loss of a phenyl end-group (e.g., \*2-DS<sub>9</sub>;  $m/z = 1187.0$ ) (*vide infra*).

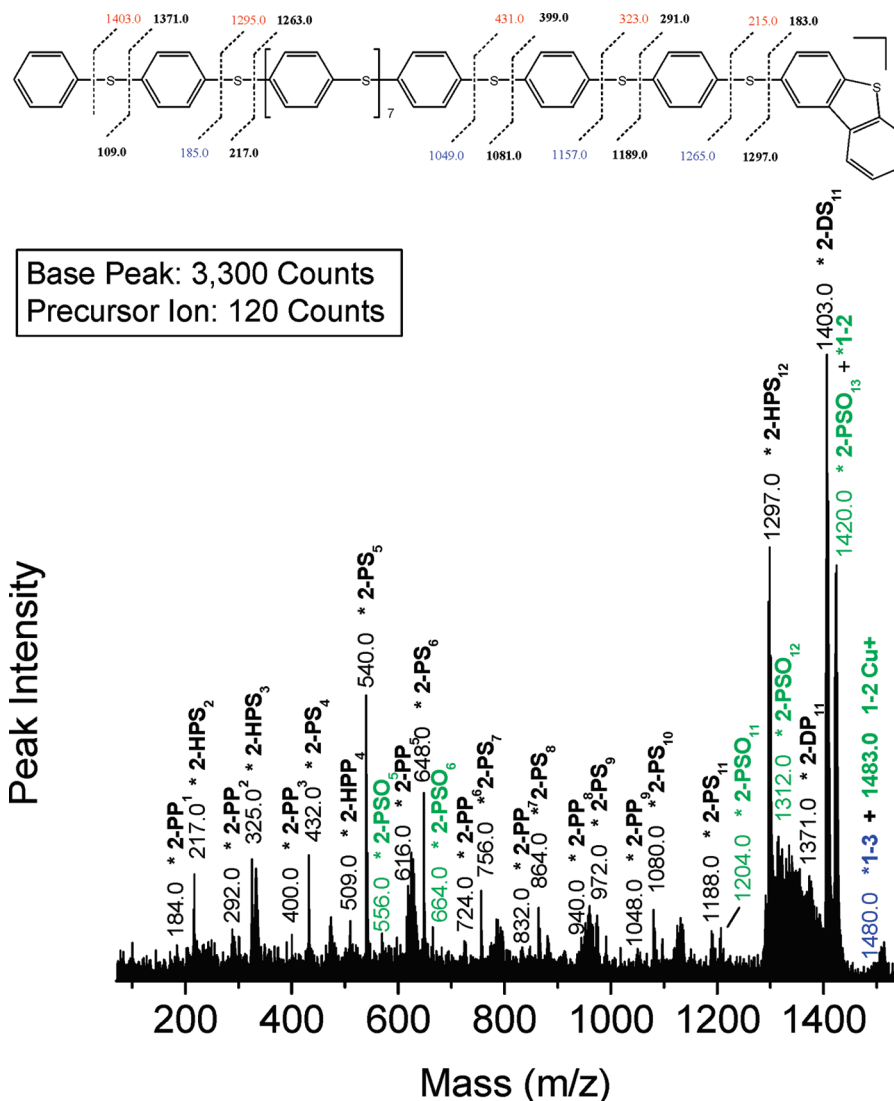


**Figure 5.** MALDI-TOF/TOF mass spectrum for dibenzothiophene–phenyl-capped linear PPS species 1–3 (1480.0 Da precursor ion) at a low collision gas pressure:  $1.5 \times 10^{-6}$  Torr. Precursor ion cationization is through carbocation formation. There is also a small portion of copper cationized species 1–2 present in the spectrum. Please note that the base peak is a fragment ion peak (1403.0 Da), produced by loss of a phenyl end-group from the precursor ion ( $M - 77$  Da). This mass spectrum has *not* been cropped.

It is also worth noting that the three diffuse peaks with center masses of approximately 391.0, 708.0, and 882.0 Da are the products of metastable ion fragmentation. They primarily appear in the CID fragmentation spectra of linear PPS (cf. Figures 2 and 4), and their peak intensities are related to the effective kinetic energy experienced by the precursor ion—compare the broad peaks in Figure 4 with those of Figures 3 and 5. However, we were unable to use the molecular mass information from these metastable fragments to gain additional insight into PPS fragmentation.

**PPS Precursor Species 1–3.** Figures 5 and S2 show MALDI-TOF/TOF CID spectra for linear dibenzothiophene–phenyl-capped species of PPS (species \*1–3: 1480.0 and 1696.0 Da, respectively). Dibenzothiophene end-groups are expected to produce unique fragmentation patterns, since they draw electron density away from the adjacent dibenzothiophene–sulfur bond—making it a weak link in the PPS chain. Furthermore, the dibenzothiophene and phenyl end-groups, on a charged species \*1–3 molecule, have the ability to disrupt resonance stabilization on their adjacent Ph–S bonds. Because of this bond weakening effect, we would expect two weak links to be introduced into the precursor ion

(e.g., Scheme 1B). If these assumptions are correct, we would expect to observe two intense fragment ion peaks at  $M - 77$  Da and  $M - 183$  Da. Also, since we are dealing with a linear species, we would expect the precursor ion to be much smaller than that observed in the CID spectra for cyclic PPS (Figures 2 and S1).

To verify our assumptions, we will first focus on the two most intense peaks in Figure 5: (1) the base peak at 1403.0 Da represents loss of a phenyl group ( $M - 77$  Da) and is consistent with our fragmentation scheme shown in Scheme 1Bi, and (2) the second most intense peak at 1297.0 Da is consistent with a  $M - 183$  fragment ion which would be produced by fragmentation of the Ph–S bond adjacent to a dibenzothiophene end-group (Scheme 1Bii). This predictable fragmentation pattern, of the end-group weakened bonds, shows great promise as a simple, yet powerful, diagnostic tool in the end-group analysis of PPS—regardless of the presence of isobaric species.

Next, we will once again use a species specific fragmentation mechanism, located at the top of Figure 5, to analyze the fragmentation spectrum and identify the chemical structure

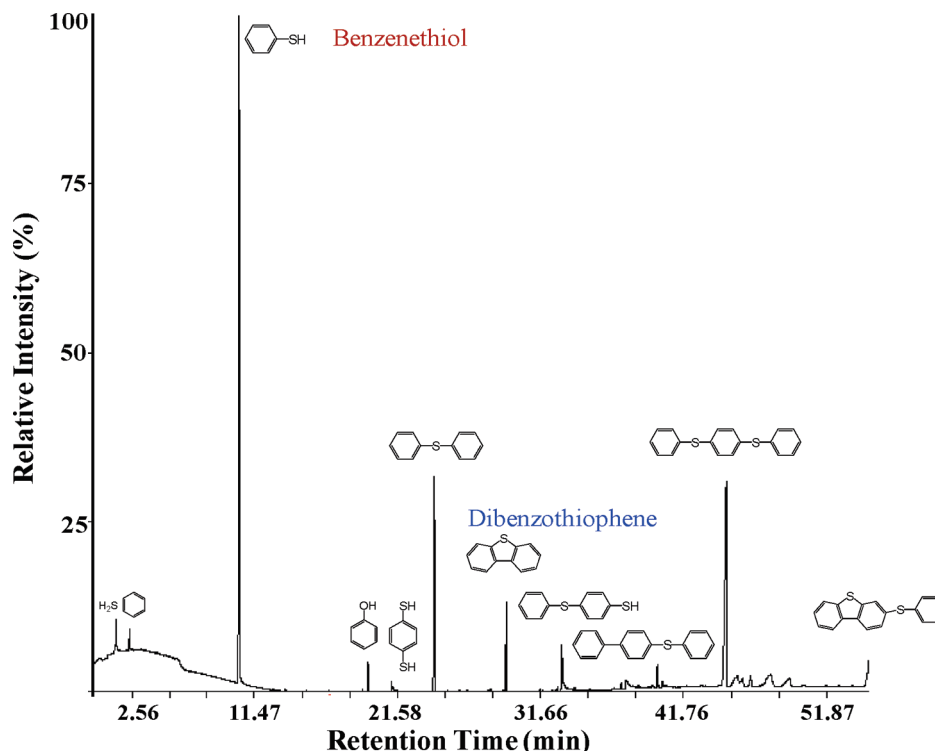


**Figure 6.** Py-GC/MS pyrogram of 0.5 mg of poly(*p*-phenylene sulfide) taken at 650 °C.

of the precursor ion—in this case a linear dibenzothiophene–phenyl-capped species. Working from left-to-right (the bottom row of mass numbers), through the predicted fragment ions in Figure 5, we can identify peaks at  $m/z$  = 184.0 (\*2-PP<sub>1</sub>), 217.0 (\*2-HPS<sub>2</sub>), 292.0 (\*2-PP<sub>2</sub>), 325.0 (\*2-HPS<sub>3</sub>), 400.0 (\*2-PP<sub>3</sub>), 432.0 (\*2-PS<sub>4</sub>), 509.0 (\*2-HPP<sub>4</sub>), 540.0 (\*2-PS<sub>5</sub>), 572.0 (\*2-SS<sub>5</sub>), 616.0 (\*2-PP<sub>5</sub>), 648.0 (\*2-PS<sub>6</sub>), 724.0 (\*2-PP<sub>6</sub>), 756.0 (\*2-PS<sub>7</sub>), 832.0 (\*2-PP<sub>7</sub>), 864.0 (\*2-PS<sub>8</sub>), 940.0 (\*2-PP<sub>8</sub>), 972.0 (\*2-PS<sub>9</sub>), 1048.0 (\*2-PP<sub>9</sub>), 1080.0 (\*2-PS<sub>10</sub>), 1156.0 (\*2-PP<sub>10</sub>), 1188.0 (\*2-PS<sub>11</sub>), 1264.0 (\*2-PP<sub>11</sub>), and 1297.0 (\*2-HPS<sub>12</sub>; M-183 Da). A summary of these fragment peaks is presented in Table 3 for comparison with fragment ions observed in Figures 2–5 and S2. Similarly, working from right-to-left (the top row of mass numbers), notable fragment peaks include are identified at  $m/z$  = 1371.0 (\*2-DP<sub>11</sub>) and 1403.0 (\*2-DS<sub>11</sub>).

Trace quantities of species 1-2 are also identified in Figure 5. However, the sulfoxide-containing fragments (labeled \*2-PSO) are much less intense than those observed in Figure 4. Also, note that the M–Cu<sup>+</sup> peak, the fingerprint peak for species 1-2 Cu<sup>+</sup>, is much less intense than that observed in Figure 4. Further, this peak is completely absent in Figure S2, indicating that the sulfoxide formation in cyclic PPS is confined to the lower molecular weight portion of this sample, in this case below 1300 Da.

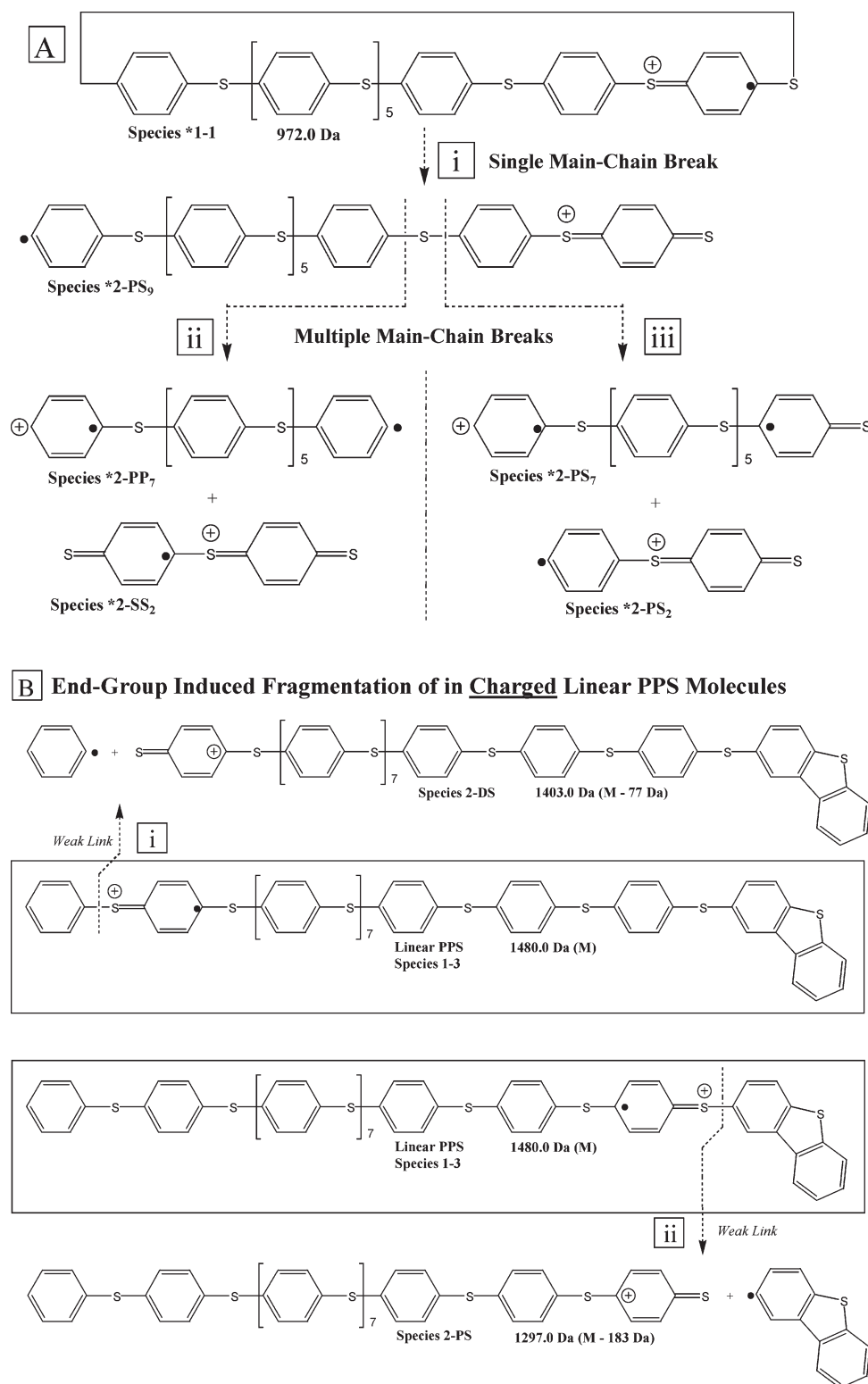
Inspection of the fragment species present in Figures 5 and S2 reveals that \*2-PS and \*2-PP produce the major fragment ions observed during CID fragmentation of linear PPS. It should also be noted that no fragment ion peaks were observed for the less stable sulfur–sulfur capped species (\*2-SS), as previously observed in Figures 2 and S1. A rationale explanation of this would be that higher molecular weight precursor ions can dissipate kinetic energy through translational motion and short-chain monomer reversion, as shown in Scheme 2D, to produce more stable \*2-PS and \*2-PP species. Additionally, the secondary reactions shown in Scheme 2B, followed by short-chain monomer reversion,

would suppress the appearance of \*2-SS fragments in the CID fragmentation spectra.

**Pyrolysis-GC/MS.** An important question is whether studies of polymer pyrolysis in the condensed phase can provide insights into the mechanisms for PPS predicted by MALDI-TOF MS (using selective extraction techniques)—ultimately leading to ways in which decomposition might be inhibited to form more thermally stable high polymers. We will first present the terminology for describing the pyrograms, and then we will present a comparison of Py-GC/MS with MALDI-TOF MS to further validate our findings from MS/MS.

The following terminology will be used when relating the pyrolysis products in Table 4 with their peak intensities observed in the PPS program shown in Figure 6: major (> 50% base peak, BP: only one is observed); medium (30–50% BP); small (7–30% BP); minor (3–7% BP); and trace (< 3% BP). In the following section, we will discuss the observed pyrolysis product peaks in decreasing order of peak intensity (i.e., major, medium, small, minor, and trace).

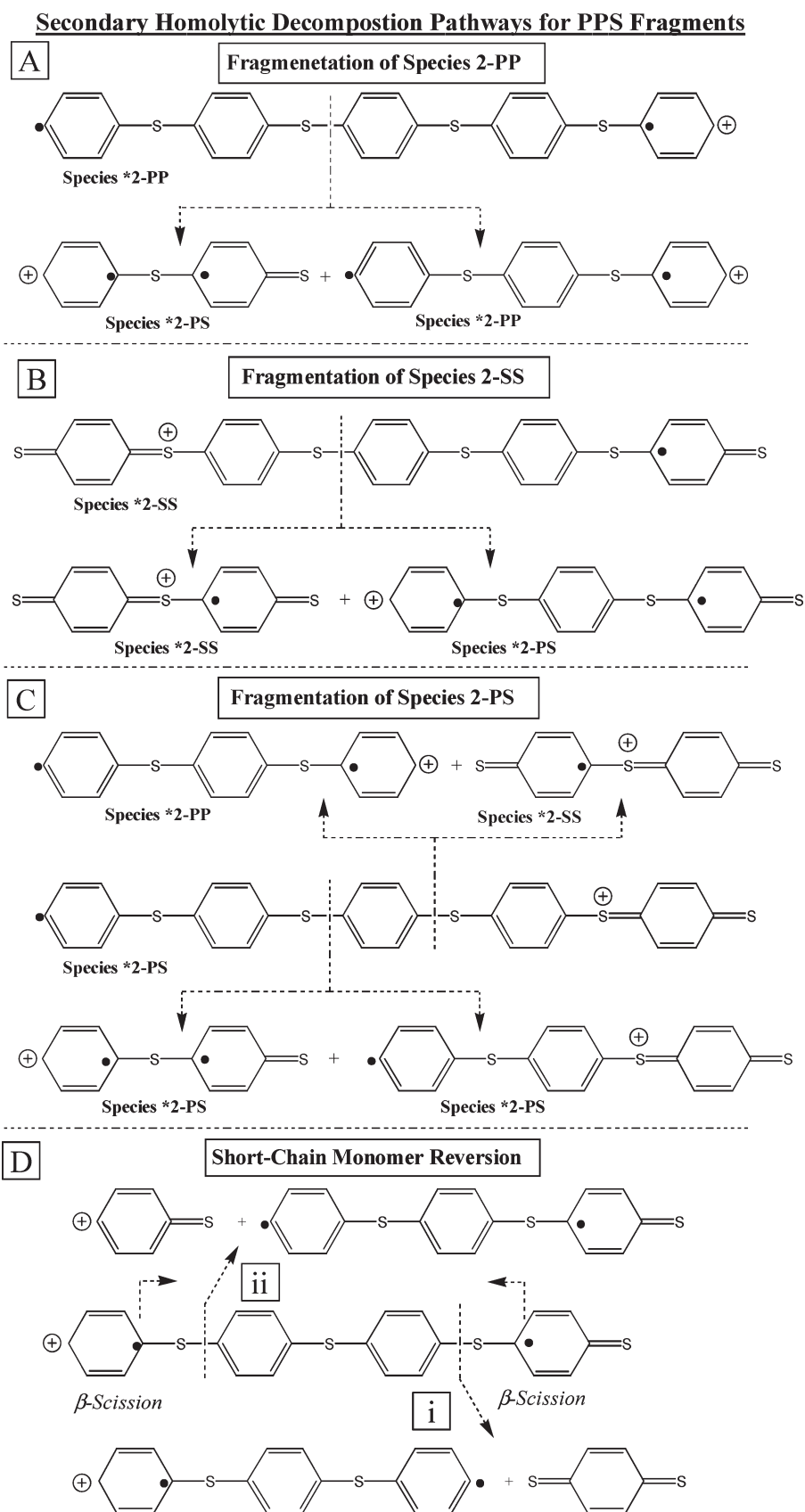
*Similarities between MALDI-TOF/TOF CID Fragmentation and Py-GC/MS Data.* The predominance of benzenethiol (species 4-1), the major species identified in Figure 6, can be explained by multiple main-chain fragmentation and short-chain monomer reversion. This process is shown in Scheme 4 and is consistent with the fragmentation mechanisms previously described in Schemes 1–3. Initial homolytic cleavage of the phenyl–sulfide backbone, in the “precursor” chain, creates two shorter (“product”) chains: one terminated with a phenyl radical and another with a sulfenyl radical. The phenyl radical can undergo a number of  $\beta$ -scissions (as shown in Scheme 4A) to form benzenethiol (the major species observed in the program, Figure 6), while the sulfenyl radical (shown in Scheme 4B) can transfer the radical into the nearby benzene ring, where it is stabilized until it occupies the para-position (relative to the

Scheme 1. Initial Bond-Breaking Mechanisms for PPS<sup>a</sup>

<sup>a</sup> (A) cleavage of a single Ph–S bond (i), followed by multiple Ph–S main-chain bond cleavages (ii and iii) for production of fragment species 2-PP, 2-PS, and 2-SS and (B) end-group-induced fragmentation in linear dibenzothiophene–phenyl-capped PPS, which yield (i) M-77 Da and (ii) M-183 Da fragment ions.

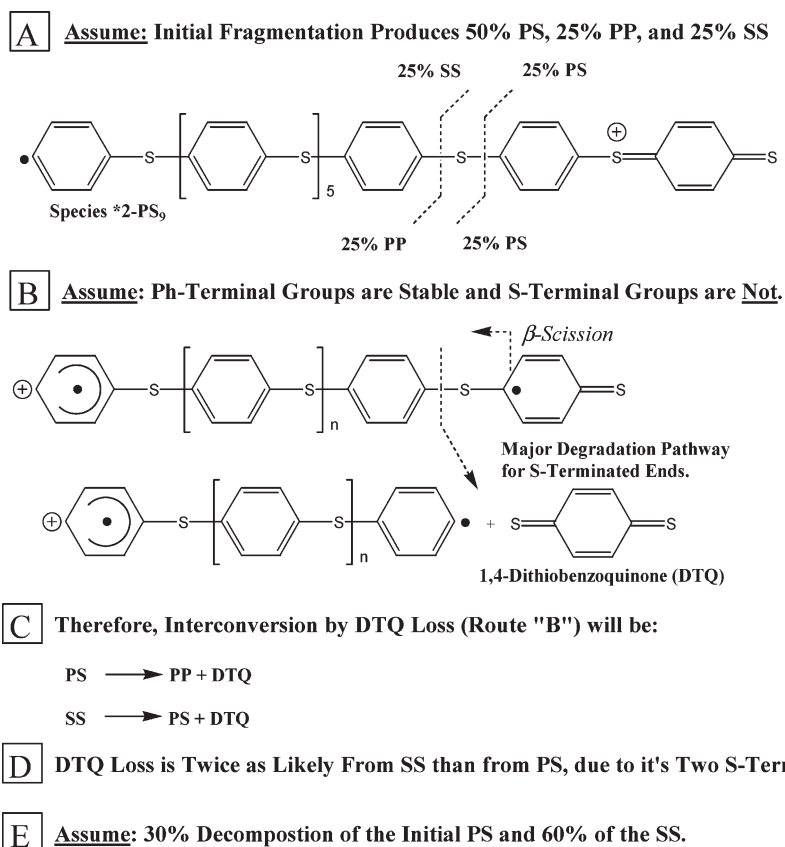
sulfur group) and initiates  $\beta$ -scission: leading to 1,4-benzenedithiol (species 4-13: a trace peak in Figure 6) and a phenyl radical. This phenyl radical can now feed back into the mechanism shown in Scheme 4A and undergo  $\beta$ -scission reactions to produce more benzenethiol (species 4-1).

Secondary reactions, such as random main-chain breaks followed by hydrogen abstraction (Scheme S1A in the Supporting Information) explain the appearance of the medium intensity peaks for diphenyl sulfide (species 4-2) and 4-(phenylthio)-diphenylsulfide (species 4-3). Since high-MW PPS is synthesized using a slight excess of dichlorobenzene, we

Scheme 2. Secondary Fragmentation Mechanisms of PPS Fragment Species<sup>a</sup>

<sup>a</sup> (A) fragmentation of species \*2-PP to produce species \*2-PS and \*2-PP; (B) fragmentation of species \*2-SS to produce species \*2-PS and \*2-SS; (C) fragmentation of species \*2-PS to produce species \*2-PP, \*2-SS, and \*2-PS; and (D) short-chain monomer reversion to produce (i) neutral species 2-SS<sub>1</sub> and (ii) species \*2-PS<sub>1</sub>. These mechanisms are in agreement with the suppressed appearance species \*2-SS in Figures 2–5, S1, and S2.

Scheme 3. Interconversion of PP, PS, and SS Species



would expect to see a preference for phenyl-capped monomers and dimers during random main-chain fragmentation. Lesser secondary reactions, such as random main-chain scission followed by phenyl radical recombination (Scheme S1B), explain the trace peaks observed for biphenyl (species 4-15) and biphenylthiol (species 4-16). Because of their intensities, the peaks for 4-(phenyl)diphenyl sulfide (species 4-9) and 2-(phenyl)dibenzothiophene (species 4-11) appear problematic, if we were to only consider the pyrolysis phenyl radical recombination mechanism. However, when arylthio metathesis reactions, previously reported by Fahey and Ash,<sup>22</sup> are considered, species 4-9 and 4-11 can be attributed groups present in the intact polymer backbone and not simply secondary reactions from pyrolysis.

The small peaks (in Figure 6) for dibenzothiophene (species 4-4) and 2-(phenylthio)dibenzothiophene (species 4-6) could be explained by a cyclization mechanism (Scheme S2) previously described by Perng,<sup>11</sup> along with the trace peaks for 3-thiobenzothiophene (species 4-12) and 2-(phenyl)dibenzothiophene (species 4-11). Comparison of the peak intensities of the cyclic dibenzothiophenes (species 4-4, 4-6, 4-11, and 4-12) with those of their linear counterparts (species 4-2, 4-3, 4-9, and 4-5, respectively) reveals that the cyclic ("product") peaks are approximately one-half to one-fourth the peak intensity of their linear ("parent") peaks. The peak intensities of the dibenzothiophenes (especially, species 4-4 and 4-6) are again consistent with high-MW PPS synthesized with a slight excess of dichlorobenzene; the phenyl-capped dimer and trimer are

the most intense peaks. Considering that linear dibenzothiophene-phenyl-capped species (species 1-3) were identified in our MALDI-TOF mass spectra by CID fragmentation (Figures 4 and 5), we must concede that a small portion of these peak intensities are from dibenzothiophene linkages being present in the polymer. However, the majority of the dibenzothiophene species, identified by pyrolysis, are formed through secondary cyclization reactions. Further, there appears to be competition between hydrogen abstraction and cyclization (e.g., dibenzothiophene formation) after main-chain scission, with H-abstraction being favored.

The minor phenol (species 4-8) peak, in Figure 6, can be explained as being a product of the sodium *N*-methyl-2-aminobutanoate (SMAB)/PPS reactions previously reported by Fahey and Ash.<sup>22,23</sup> Furthermore, when considering the presence of phenol groups and their importance in the speed of PPS curing, the excess dichlorobenzene used in the synthesis will yield a predominance of chlorobenzene-capped PPS chains. This presents a problem for thermal curing: two chlorobenzenes will not undergo chain-extension reactions with each other. However, when a few hydroxyl groups replace some of the chlorobenzene end-groups, the chain-extension reactions can readily proceed through the formation of ether linkages, a stable bond in high temperature aromatic polymers.

Finally, it is interesting to note that the sulfoxide linkage (species 1-2) identified by CID fragmentation (Figure 4) was not identified by pyrolysis (Figure 6). There are two plausible explanations for this: (1) the sulfoxide-containing cyclics



- (21) Gies, A. P.; Vergne, M. J.; Orndorff, R. L.; M., H. D. *Anal. Bioanal. Chem.* **2008**, *392*, 609–626.
- (22) Fahey, D. R.; Ash, C. E. *Macromolecules* **1991**, *24*, 4242–4249.
- (23) Fahey, D. R.; Hensley, H. D.; Ash, C. E.; Senn, D. R. *Macromolecules* **1997**, *30*, 387–393.
- (24) Almén, P.; Ericsson, I. *Polym. Degrad. Stab.* **1995**, *50*, 223–228.
- (25) Perng, L. H. *J. Polym. Sci., Part A: Polym. Chem.* **2000**, *38*, 583–593.
- (26) Perng, L. H. *J. Polym. Sci., Part A: Polym. Chem.* **2001**, *81*, 2387–2398.